# ZINC OXIDE: SURFACE STRUCTURE, STABILITY, AND MECHANISMS OF SURFACE REACTIONS

# M. GRUNZE, W. HIRSCHWALD and D. HOFMANN

Institute of Physical Chemistry, Free University of Berlin Takustrasse 3, D-1000 Berlin 33 (Dahlem), West-Germany

Surfaces of ZnO are characterized by surface spectroscopical techniques, LEED, SEM, etching (thermal and chemical), vaporization, and photodecomposition. The interaction of these surfaces with oxygen, hydrogen, and water is also investigated.

### 1. Morphology and surface structure

The best method to obtain large, perfect, and reasonably pure ZnO single crystals is, presently, a CVD process making use of reduction/oxidation equilibria. A mixture of nitrogen and hydrogen is passed over ZnO at elevated temperatures, and the redeposition and crystal growth occurs at the same or slightly lower temperatures. The wurtzite-type crystals grown by this process exhibit well defined principal faces,  $(000\overline{1})$  and  $(10\overline{1}0)$  [1], as indicated schematically in fig. 1. The polarity along the c-axis is shown by the lattice model of fig. 2 which shows that planes of zinc ions alternate with planes of oxygen ions.

Characterizing these crystal surfaces by AES, LEED, and XPS reveals that they are clean and that they carry much less than a monolayer of adsorbed contaminants after cleavage in air (mainly carbon, sulfur, and chlorine), fig. 3a. This

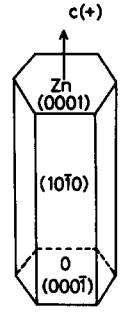


Fig. 1. Schematic characterization of the principal faces and anisotropy of ZnO single crystal.

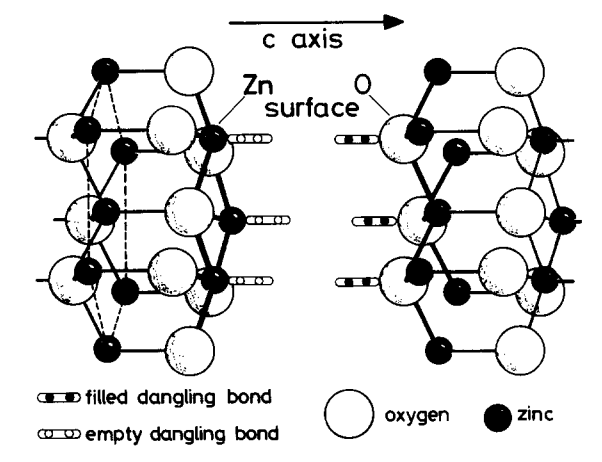
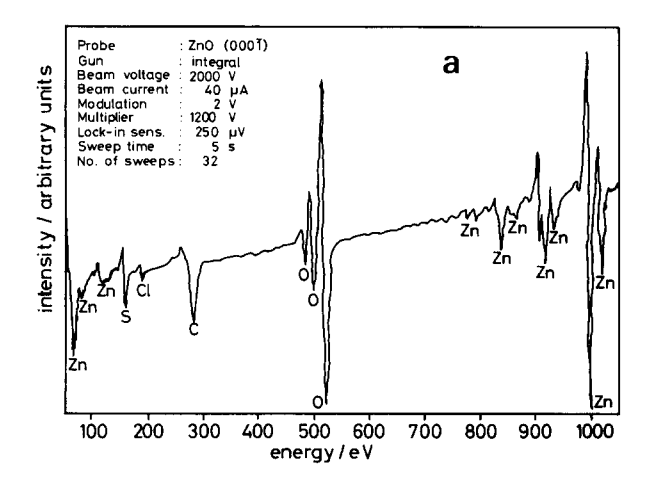


Fig. 2. Lattice model of ZnO demonstrating the nonstoichiometry of polar faces and surface dangling bonds [2].

can be removed by a slight argon ion bombardment of monolayer dosage, fig. 3b. After this cleaning procedure a clear  $1 \times 1$  LEED structure can be seen on both polar faces, fig. 4, a faint indication of which can already be seen before the cleaning procedure. Heating the crystal up to 900 K in ultra-high vacuum leads to faceting and step formation on the surface, fig. 5. Overlayer structures can only be observed in connection with contaminations; for example, potassium from filaments of the UHV equipment lead to a  $2\sqrt{3} \times 2\sqrt{3}$  structure, fig. 6, which disappears simultaneously with the removal of the contamination by thermal annealing.

In general, no pronounced difference was observed by AES and LEED for the two polar faces. XPS reveals a slightly higher electron



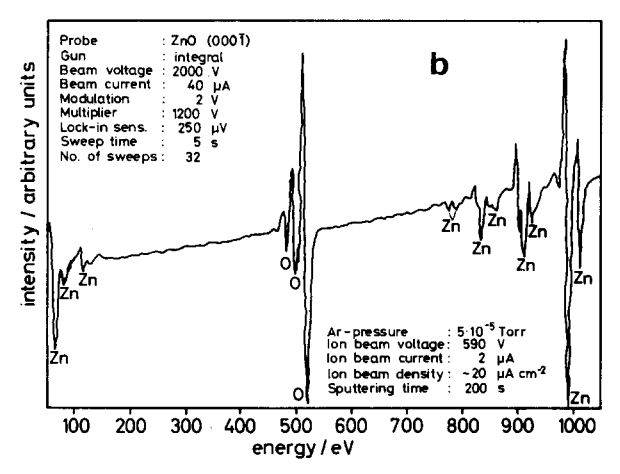


Fig. 3. Auger electron spectra (AES) of  $(000\overline{1})$ ZnO face: (a) after cleavage in air, as mounted in UHV; (b) after slight argon ion bombardment (about 1 L).

population at the low energy edge of the Zn 3d band on (0001)Zn, fig. 7, an effect which can be attributed to the different bonding states of zinc ions on both faces, but which also might simply be due to a shielding effect of oxygen ions on (0001)O.

More pronounced differences in the polar behaviour of the (0001)Zn and (0001)O faces can be clearly observed on a macroscopic scale by chemical and thermal etching, dissociative evaporation, photodecomposition, initial surface conductivity, and other effects some of which will be illustrated in the following by some micrographs and diagrams. Chemical etching by

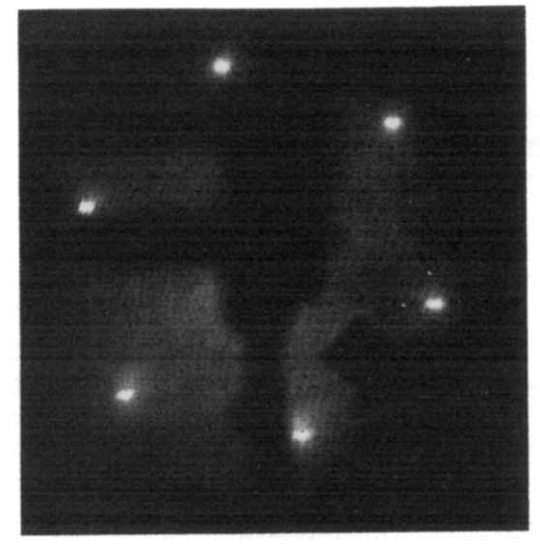


Fig. 4.  $(1 \times 1)$  LEED pattern of  $(000\overline{1})$ ZnO face after pretreatment according to fig. 3b.

hydrofluoric acid (20 min, 40%) reveals a more severe and more localized attack on  $(000\bar{1})O$ than on (0001)Zn [4]. A roughly 2000-fold magnification of the markedly affected  $(000\bar{1})O$ face, fig. 8, exhibits facets of  $(110\overline{1})$  type by SEM, while on the mainly smooth (0001)Zn face only sparsely distributed hexagonal etch pits can be seen, fig. 9. HF-etching on (1010) faces produce arrows pointing with their tip in the positive c-direction, an observation that provides an easy identification of the polar faces, as was first pointed out by Klein [4]. Thermal etching (10 h, 1270 K) reveals morphologic features, similar to chemical etching, fig. 10, again exhibiting markedly different patterns for (0001) and  $(000\overline{1})$ . Due to different surface relaxation, morphology, and specific (active) surface area the steady-state rate of dissociative evaporation is different for both faces [6]. However, in the monolayer range of decomposition, a transient behaviour, again distinctly different for the two polar faces, is observed, fig. 11. After cleavage of ZnO single crystals perpendicular to the c-axis in UHV at 100 K, initial heating in UHV reveals an onset of zinc desorption from the (0001) face at 655 K. The process, observed by mass spectrocopy and sheet conductance comes to completion after one monolayer has been desorbed at this tem-

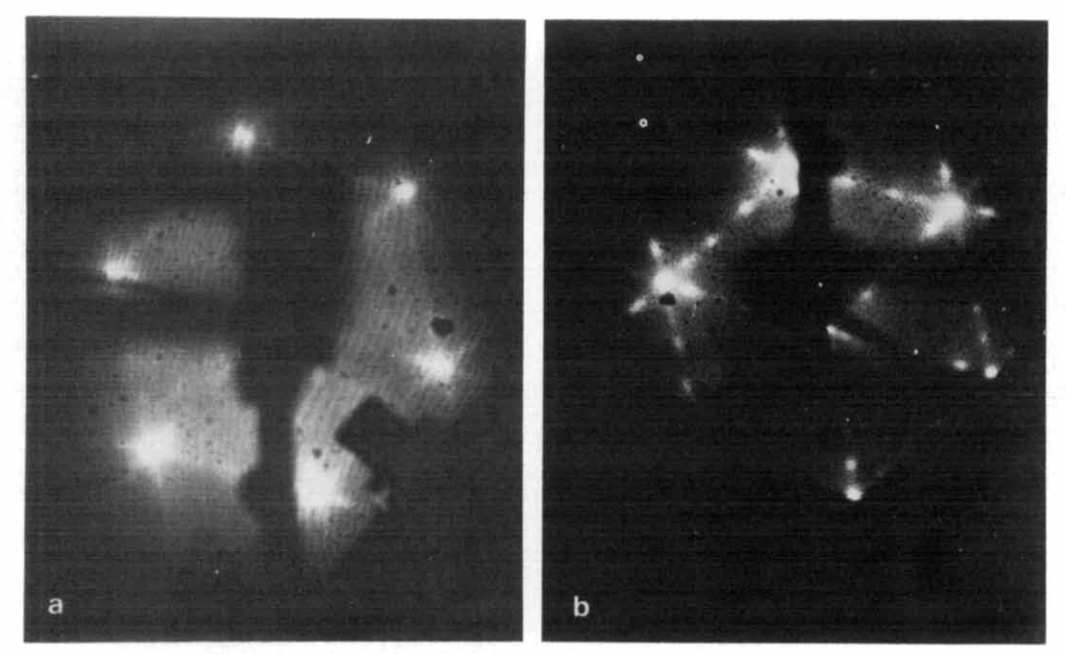


Fig. 5. LEED pattern of  $(000\overline{1})$ ZnO revealing faceting and step formation after thermal annealing in UHV: (a) 120 min, 900 K; (b) >150 min, 900 K.

perature. On (0001) the onset of evaporation of lattice constituents is observed only at 875 K [7]. Surface relaxation on (0001)Zn leads to an irreversible increase in conductivity above 500 K,

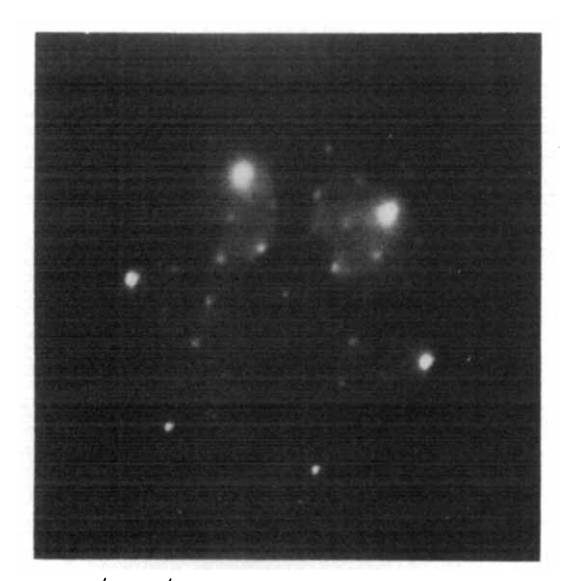


Fig. 6.  $(2\sqrt{3} \times 2\sqrt{3})$  overlayer structure caused by potassium contamination on  $(000\overline{1})$ ZnO.

while on (0001)O the sheet conductance is reversible in this temperature region [2].

# 2. Kinetics of surface reactions

Considering the CVD crystal growth process a little more in detail, fig. 12, two chemical reactions are mainly of interest: the transport reaction itself

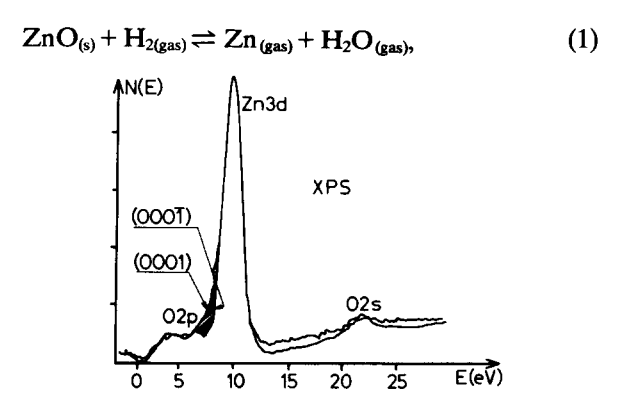


Fig. 7. XPS spectra of (0001)Zn and (0001)O faces.



Fig. 8. Scanning electron micrograph (1600×) of HF-etched (000 $\overline{1}$ ) face.

and – under conditions of incomplete backward reaction and with a slight counter stream of air (a measure applied in the technological crystal growth process) – the oxidation of zinc vapour by oxygen

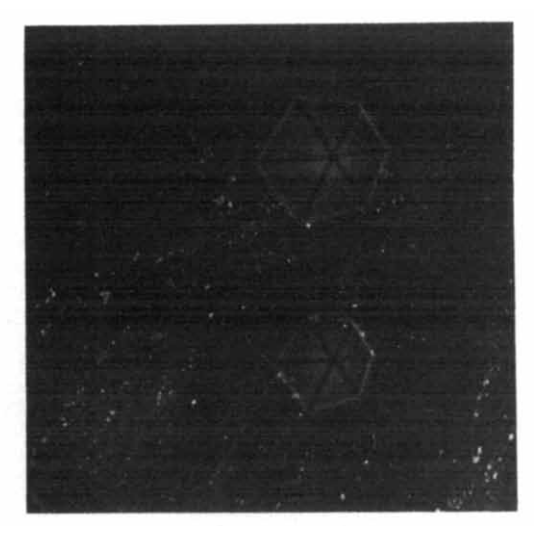


Fig. 9. Scanning electron micrograph ( $5400\times$ ) of HF-etched (0001) face.

$$Zn_{(gas)} + \frac{1}{2}O_{2(gas)} \rightleftharpoons ZnO_{(s)}.$$
 (2)

Inspection of these two processes in relation to surface properties, surface reactivity, and micro-

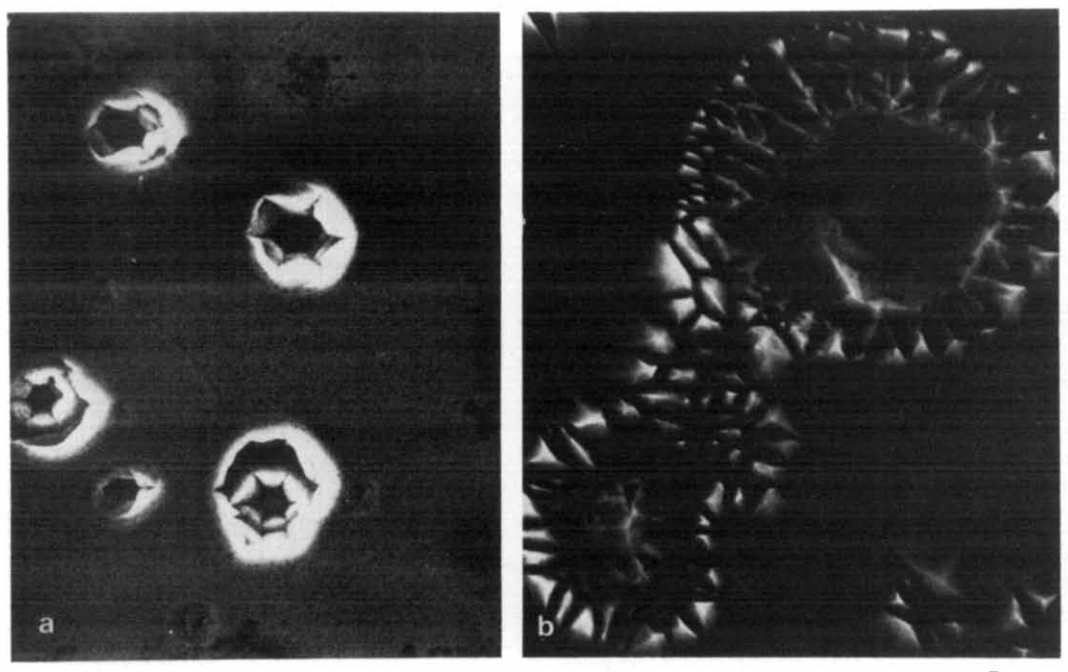


Fig. 10. Etching patterns produced by thermal annealing in vacuum (10 h, 1270 K): (a) (0001),  $1900 \times$ ; (b) (000 $\overline{1}$ ),  $2400 \times$ .

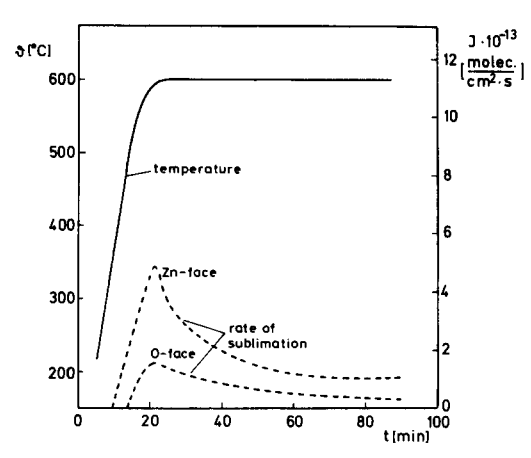


Fig. 11. Non-steady-state rate of dissociative sublimation in the monolayer range during initial heating of oxygen-treated polar faces in UHV.

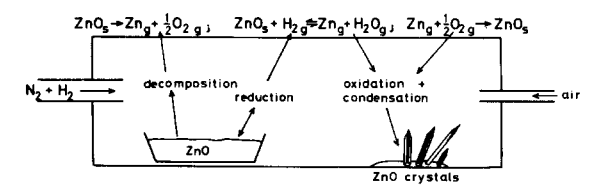


Fig. 12. Schematic representation of ZnO single crystal growth process by CVD and basic reactions.

growth and micro-decomposition processes reveals some interesting and even unique patterns. terns.

#### 2.1. Reactions with oxygen

Starting from the oxidation/decomposition equilibrium (2), the diagram of state, as well as vaporization experiments [5, 8], show that the phase transition solid  $\rightarrow$  gas occurs via decomposition. Recent mass spectrometric investigations, using a Knudsen cell arrangement, demonstrate that the contribution of  $ZnO_{(gas)}$  molecules to the evaporation/transportation process is negligible, in spite of a considerable Zn-O bond energy of 256 kJ/mole taken from the temperature dependence of  $I_{ZnO}$  [9].

An explanation for the dissociative evaporation can be derived from the lattice structure, the degree of ionicity ( $\approx 1$ ), and the magnitude of the band gap  $E_g$  ( $= 3.2 \, \text{eV}$ ). In order to remove a

ZnO molecule from the solid surface, three zinc/oxygen bonds have to be broken, while for dissociative evaporation the fission of only two bonds is necessary. If ions were desorbed from the surface, the long range Coulombic contribution would be large and would not necessarily favour dissociative vaporization, as in the case of NaCl, for instance, which has a high ionicity and a comparatively large gap. In ZnO ionicity and gap energy are smaller so that neutralization by change transfer:

$$(Zn^{2+}O^{2-})_s + 2(e \sim h) \rightarrow (Zn^0O^0)_s,$$
 (3)

preceding separation and desorption, requires less energy ( $\approx E_{\rm gap}$ ). In an earlier study we were able to show that electron transfer from the O 2p valence band to the Zn 4s conduction band, corresponding to neutralization, is the step with the highest energy requirement in the sequence of stepwise vaporization. Consequently, the band gap energy was found to be about equal to the activation energy of vaporization, as taken from our Langmuir experiments [5]. This observation shows that photodecomposition of solid zinc oxide surfaces by band-to-band excitation should be possible. Corresponding experiments in an UHV mass-spectrometric system revealed a photostimulation of ZnO decomposition [10].

As can be seen from fig. 13, photodecomposition is a transient effect, obviously due to the action of zinc atoms or clusters as recombination centres. This conclusion is derived from the fact that photodecomposition is observable only at

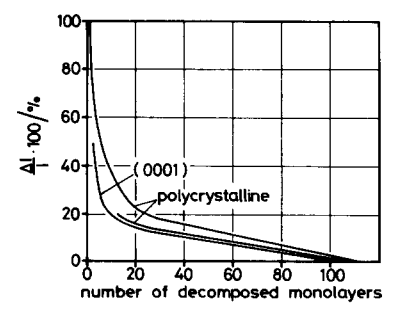


Fig. 13. Relative increase of transient decomposition of oxygen-treated ZnO surfaces by UV photostimulation versus numer of decomposed monolayers [11].

temperatures high enough for zinc desorption (>600 K). Furthermore, enrichment of zinc interstitials Zn<sub>i</sub> in the near-surface region enhances recombination by providing an accumulation of electrons near the surface,

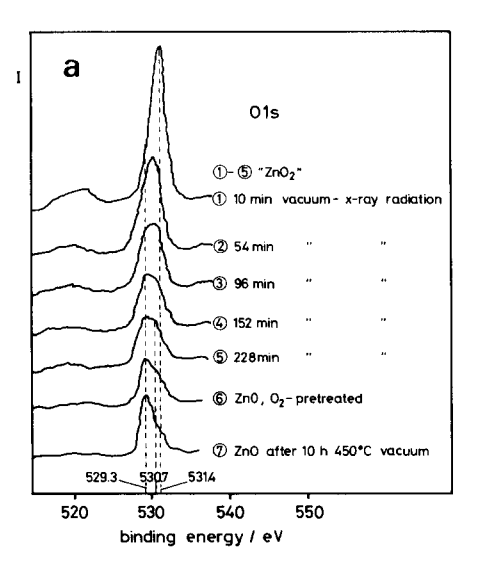
$$Zn_i \to Zn_i^+ + e^-. \tag{4}$$

For an efficient photoeffect another condition has to be fulfilled: electron-hole pairs (excitons) have to be separated to avoid instantaneous recombination. This can be achieved by generating pairs in a gradient of the electrical field which is established by acceptor adsorption on the ntype semiconductor zinc oxide. It is well known that oxygen chemisorption leads to depletion layers on zinc oxide and strong band bending. This situation is especially favourable for lattice decomposition as holes are attracted to the negatively charged surface, thus neutralizing lattice oxygens in kink positions and enabling them to desorb. Likewise, electrons are repelled towards the interior and able to neutralize zinc ions.

Finally, enrichment zinc (i.e. nonstoichiometry), due to incomplete desorption that occurs during photodecomposition, has a pronounced effect on the structure of the space charge layer and the effectiveness of charge separation. On zinc-rich surfaces covered with an acceptor gas, the extension  $\delta$  of the space charge layer is in the range of some angströms (quasimetallic), and it is much smaller than in oxygen treated nearly stoichiometric crystals for which  $\delta \simeq 10^{-5}$  cm. As the penetration depth of 3.2 eV photons is in the range of some 10<sup>-5</sup> cm, most photons (>90%) will generate pairs in a fieldfree region in the first case, and these are ineffective for photodecomposition.

Taking into account that n-type conductivity, as always found in ZnO, is due to zinc abundance in the lattice, one can conclude from the above mentioned observations that the solid is stabilized towards thermal- and photodecomposition by slight stoichiometry deviations (≈100 ppm). O 1s and Zn 3d XPS spectra support this assumption as the binding energies of electrons are decreased for O 1s and increased

for Zn 3d by up to 2 eV, fig. 14. Direct evidence for lattice stabilization by slight stochiometry deviations is given by the investigations of oxygen decomposition pressures over solid zinc oxide [13]. As can be seen in fig. 15, the relative oxygen pressure decreases with time and temperature of vacuum annealing. Oxygen interaction at temperatures high enough for zinc migration leads to the formation of nearly stoichiometric layers with decreased stability. The change of physical properties is seen, for example, in the reflectivity curves after treatment in air at different temperatures, fig. 16. Not only is the intensity markedly changed, but the maximum is also shifted to smaller wavelengths [14].



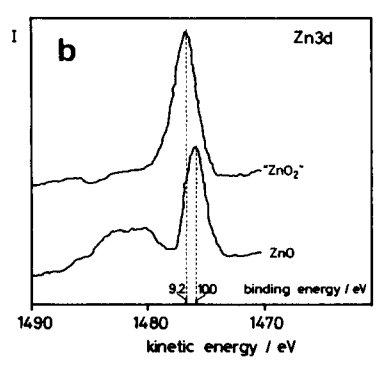


Fig. 14. XPS spectra of hydroperoxide ("ZnO<sub>2</sub>"), oxygen, and vacuum-treated/annealed ZnO surfaces: (a) O 1s peak [11]; (b) Zn 3d peak, in the course of vacuum annealing.

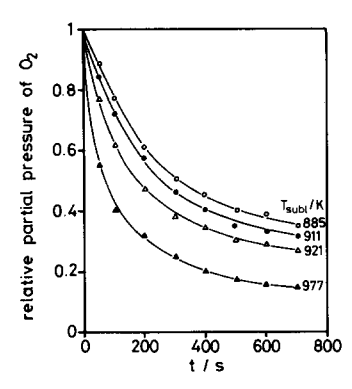


Fig. 15. Lattice stabilization by oxygen release leading to zinc abundance. Decrease of  $(p/p_0)_{O_2}$  during initial heating of oxygen annealed  $(10\overline{1}0)$  faces [13].

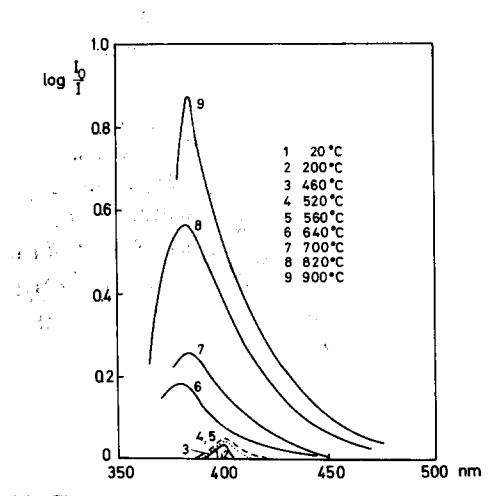


Fig. 16. Changes of reflectivity of polycrystalline ZnO surface by annealing in air at different temperatures [14].

SIMS for both states (zinc-rich and oxygen-rich) shows that Zn and Zn<sub>2</sub> intensitites are more pronounced in the zinc-rich case, fig. 17, and this additional intensity decreases with increasing sputter time. Oxygen-containing fragments like  $ZnO_2^-$  and  $ZnO_3^-$  are pronounced in the negative spectra, fig. 18, giving evidence to the type of coordination in the ZnO lattice.

The degree of nonstoichiometry, i.e. the surface concentration of point defects (zinc interstitials or oxygen vacancies), not only influences the stability of the surface but also its chemisorptive and catalytic activity, as was pointed out and intensively investigated for  $(10\overline{10})$  faces by Göpel [13, 15, 16]. Changes in surface electron

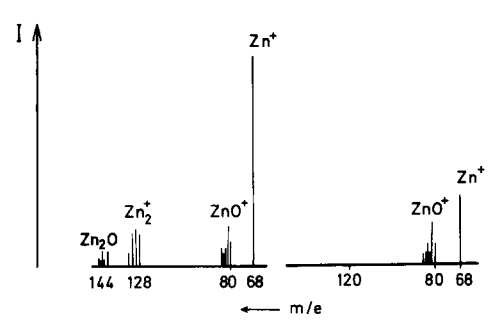


Fig. 17. Comparison of secondary ion mass spectra (SIMS) of zinc rich (left) and nearly stoichiometric (right)  $(10\overline{10})$  face.

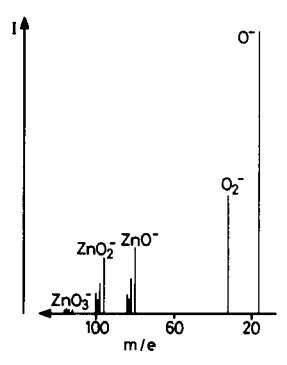


Fig. 18. Spectrum of negative ions from (1010) face.

concentration by a factor of 10 and a decrease of mobility by a factor of 0.5 are observed after UHV treatment above 700 K. Surface concentration of defects are in the range of  $10^{-3}$  to  $10^{-2}$ [16]. Corresponding to the surface defect concentration, the sticking coefficient of oxygen is distinctly changed, fig. 19. The exponential increase of  $S_0$  in the low temperature region (300 K) indicates the influence of band bending on oxygen chemisorption, while the linear dependence of  $S_0$  on surface defect concentration at 700 K is due to dissociative surface reactions between chemisorbed oxygen and vacancies (or zinc interstitials), e.g.

$$O_{2(\sigma)}^- + V_{O_{\sigma}}^+ \to O_{\sigma} \tag{5a}$$

or

$$O_{2(\sigma)}^{-} + V_{O_{\sigma}} \rightarrow O_{\sigma}^{-} \tag{5b}$$

The situation changes drastically when using a

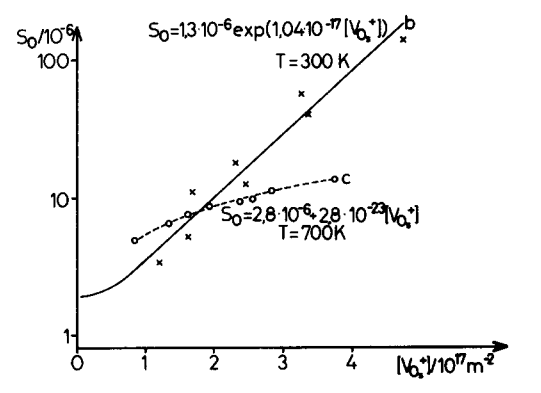


Fig. 19. Sticking coefficient  $S_0$  for  $(10\overline{1}0)$  versus surface vacancy concentration at 300 and 700 K [16].

covalent bonded gas such as CO<sub>2</sub> instead of oxygen, an acceptor gas. Effective surface reconstruction with an assumed two-dimensional "ionic→covalent" phase transition results in sticking coefficients close to unity [17].

The evaporation rates in the low temperature, non-steady-state region mentioned above indicated a dependence on stoichiometry deviation, i.e. the stability of the lattice is correlated with the concentration of point defects. This

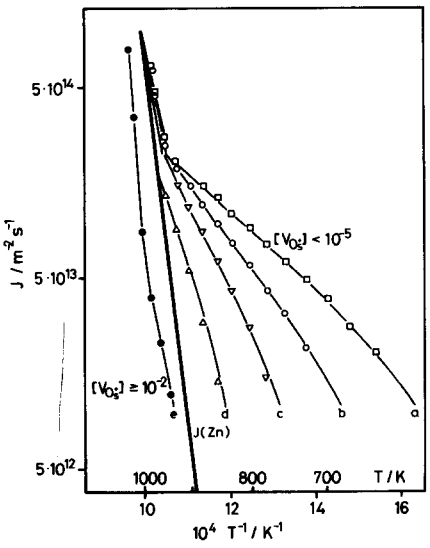


Fig. 20. Rate of oxygen release from oxygen annealed  $(10\overline{1}0)$  face versus temperature at different vacancy concentrations; (e) was obtained after sublimation at 1035 K ( $J_{(Zn)} = \text{rate of zinc desorption for comparison}) [16].$ 

correlation is quantitatively demonstrated by Göpel's studies [16], who measured the rate of oxygen removal from the lattice as a function of temperature for different surface defect concentrations, fig. 20.

# 2.2. Reactions with hydrogen

Turning to the hydrogen transport reaction, we can easily take the necessary thermodynamic information for the growth process from a plot [8] of  $\log(p_{\rm H_2O}/p_{\rm H_2})$  versus 1/T.

We gained some information concerning the hydrogen/water interaction with ZnO surfaces from thermal desorption spectroscopy (TDS), IR transmission on powders combined with electron microscopy, and from a preliminary UPS study, in addition to extensive investigations of macroscopic reduction kinetics by hydrogen and CO [3, 12, 19-21].

Long time exposure of ZnO surfaces (15 min to 20 h) to hydrogen (10<sup>-6</sup> Pa) at room temperature revealed zinc and H<sub>2</sub>O in thermal desorption spectra giving evidence for submonolayer reduction of ZnO even at room temperature [20]. This observation was confirmed by infrared transmission studies on ZnO powders after room temperature hydrogen interaction. After a short time of H<sub>2</sub> interaction (15 min,

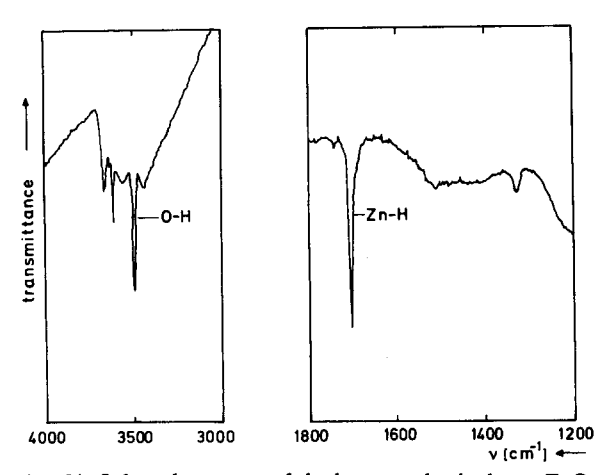


Fig. 21. Infrared spectra of hydrogen adsorbed on ZnO powder, revealing the Zn-H and O-H bands.

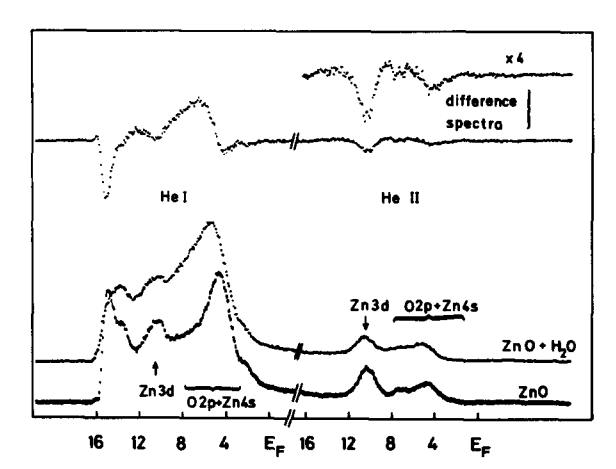


Fig. 22. He I and He II UV photoelectron spectra of clean and H<sub>2</sub>O-covered polycrystalline ZnO surfaces. Upper part: difference spectra; topmost curve: enlarged by a factor of 4.

40 mb) the well known ZnH and OH bands are observed, fig. 21, which disappear in the course of several hours, giving rise to the development of the water peak [21]. It is an interesting point that only powders exhibiting a reasonable percentage of polar faces\* (as inspected by electron microscopy) show pronounced Zn-H and O-H bands. These are probably responsible for hydrogenation processes over ZnO, and they indicate a specific catalytic activity of the polar faces for this type of reaction.

The UPS difference spectrum of chemisorbed water on ZnO indicates a possible interaction of the O 2p lone pair of the water molecule with the Zn 3d electrons of ZnO, fig. 22.

# Acknowledgement

Thanks are due to Mrs. Krebs for assistance in crystal preparation and electron microscopic inspection.

#### References

- [1] R. Helbig, J. Crystal Growth 15 (1972) 25.
- [2] G. Heiland and P. Kunstmann, Surface Sci. 13 (1969) 72.
- [3] W. Hirschwald, O. Knacke and I.N. Stranski, Z. Elektrochem. Ber. Bunsenges. 66 (1962) 29.
- [4] A. Klein, Z. Physik 188 (1965) 352.
- [5] W. Hirschwald and F. Stolze, Z. Physik. Chem. NF 77 (1972) 21.
- [6] R.B. Leonard and A.W. Searcy, J. Chem. Phys. 50 (1969) 5419.
- [7] D. Kohl, M. Henzler and G. Heiland, Surface Sci. 41 (1974) 403.
- [8] W. Hirschwald, F. Stolze and I.N. Stranski, Z. Physik. Chem. NF 42 (1964) 96.
- [9] M. Grade, W. Hirschwald and F. Stolze, Z. Physik. Chem. NF 100 (1976) 165.
- [10] M. Grunze, W. Hirschwald and E. Thull, Z. Physik. Chem. NF 100 (1976) 201.
- [11] M. Grunze, W. Hirschwald and E. Thull, Thin Solid Films 37 (1976) 351.
- [12] M. Grunze, W. Hirschwald and S. Krebs, Z. Physik. Chem. NF 102 (1976) 57.
- [13] W. Göpel, Surface Sci. 62 (1977) 165.
- [14] F. Schelfaut and W. Maenhout-van der Vorst, Photogr. Korresp. Sonderheft 8 (1966) 19.
- [15] W. Göpel, Ber. Bunsenges. 80 (1976) 481.
- [16] W. Göpel, J. Vacuum Sci. Technol. 15 (1978) 1298.
- [17] W. Göpel, J. Vacuum Sci. Technol. 16 (1979) 1229.
- [18] D. Kohl and G. Heiland, Surface Sci. 63 (1977) 96; Phys. Status Solid (a) 49 (1978) 27.
- [19] W. Hirschwald et al., Zinc Oxide Properties and Behaviour, in: Current Topics in Material Science, Vol. VII, Ed. E. Kaldis (North-Holland, Amsterdam, 1980).
- [20] E. Thull, Dissertation, Freie Universität Berlin (1976).
- [21] S. Netsch, Diplomarbeit, Freie Universität Berlin (1975).

<sup>\*</sup> These were prepared by oxidation of zinc vapour.